CIRP Journal of Manufacturing Science and Technology 10 (2015) 36–48

Contents lists available at ScienceDirect

CIRP Journal of Manufacturing Science and Technology

journal homepage: www.elsevier.com/locate/cirpj

Active vibration isolation of machine tools using an electro-hydraulic actuator

M. Law *, M. Wabner, A. Colditz, M. Kolouch, S. Noack, S. Ihlenfeldt

Fraunhofer Institute for Machine Tools and Forming Technology IWU, Department of Machine Tools and Automation, Reichenhainer Str. 88, 09126 Chemnitz, Germany

ARTICLE INFO

Article history:
Available online 15 June 2015

Keywords:
Machine tools
Active vibration isolation
Electro-hydraulic actuator
Transmissibility

ABSTRACT

This paper reports on a novel electro-hydraulic actuator that attenuates and isolates ground motion to keep dynamic excitations transmitted to machine tools below permissible levels. The first part describes the working principle of the actuator. The actuator is a classic example of a valve-controlled piston. Flow to the actuator is regulated to move the actuator and the machine that the actuator supports to compensate for ground motion experienced by the machine. Dynamics of this electro-hydraulic actuator are described in the second part of the paper. The third part describes experimental characterization of a physical prototype to identify unknown system parameters. Experimentally updated model is coupled to a virtual model of a flexible machine tool in the fourth part. Simulation driven investigations for the controlled transmissibility show the actuator to be effective in a frequency range of 1–100 Hz with case specific attenuations ranging from 5 to 25 dB. The actuator is designed with a high passive stiffness to support inertial loads of the machine. The device can be operated on demand when high precision is required, making it an energy efficient solution.

Introduction

Machine tools are often subjected to high levels of accelerations from ground motions that strain and distort the machine. This distortion depends on machine construction, machine mounting, and the amount and direction of acceleration that the machine experiences [1]. Since it is difficult to insulate the machine from its production environment or from vibration producing machines and devices, it becomes necessary to isolate the machine from such disturbances. The goal of vibration isolation is to maintain dynamic excitations transmitted to the machine to levels below the allowable machining and measurement deviations.

In most cases isolation requirements can be satisfied by judiciously designed passive isolators that have high damping and relatively small support stiffness [2,3]. Passive solutions offer design simplicity and cost-effectiveness. However, inertial excitations such as those caused by rapid positioning of drives results in undesirable residual vibrations in the form of low-frequency rocking motions of the machine on the soft passive mounts. These rocking motions degrade machine accuracy and there have been several attempts to mitigate them [1–4]. Despite the advantages of passive isolators and advances made to mitigate rocking, design of effective passive isolation mounts in situations when the ground vibrates with an unpredictable waveform that has broadband spectrum, is difficult. Since such broadband and random excitation is often the case in modern production environments, it becomes necessary to devise active isolation solutions instead.

Active isolation solutions include a feedforward and/or a feedback circuit that consists of a sensor, a controller and an actuator. Such solutions have shown to be very effective in automotive suspensions, telescopes, satellites, space, and even in seismic applications [5–8]. Actuating mechanisms in these applications include isolators that use hydraulic, pneumatic, electromagnetic, piezoelectric, and magnetorheological (MR) fluid-elastomer solutions. Small deflection capacity of piezoelectric actuators limits their use in machine tool isolation applications. Inability of pneumatic actuators to support high static and dynamic loads also limits their use in machine tool isolation solutions. Furthermore, the nonlinear force hysteresis characteristics of MR mounts combined with their high costs are factors that limit their use in machine tool isolation applications.

Competing requirements of high static stiffness required to support the large inertial load of the machine combined with low eigenfrequency requirements for effective isolation, make the

* Corresponding author. Tel.: +49 371 5397 1518.
E-mail address: mohit.law@iwu.fraunhofer.de (M. Law).

http://dx.doi.org/10.1016/j.cirpj.2015.05.005
1755-5817/

design and use of active isolators difficult in machine tool applications. Active isolators for machine tools must be sensitive to the dynamic characteristics of the machine being isolated and to the spectral and spatial characteristics of the floor vibrations. Moreover, an active solution should be able to work on demand, especially in situations where high precision is required or on a temporary basis until a more permanent and robust passive solution can be designed.

To address the above issues, a novel electro-hydraulic actuator has been developed at the Fraunhofer IWU [9]. The proposed solution builds on the first generation of such electro-hydraulic actuators reported elsewhere in [10]. The actuator is a classic example of a valve-controlled piston, as described in the Electro-hydraulic actuator working principle section. Flow to the piston is regulated to move the actuator and the machine that the actuator supports to compensate for ground motion experienced by the machine. Since vertical motions are twice as severe as horizontal ground motions [2–4], the solution presented is limited to mitigate only vertical ground motions.

Hydraulic actuators afford a high passive stiffness that can support large inertial loads without resulting in rocking. Higher hydraulic stiffness and the resulting higher natural frequency allows a faster speed of response, making possible continuous and/or intermittent operation as may be required to respond to broadband base excitation. Moreover, since most machine tools already have hydraulic aggregates as auxiliary equipment, the actuator can run on the same aggregate, allowing easier implementation.

To demonstrate how the developed electro-hydraulic actuator can isolate machine tools from ground vibrations, actuator dynamics are formulated as discussed in the Modelling the electro-hydraulic actuator dynamics section. The Experimental characterization of actuator dynamics section discusses identification of unknown model parameters. Since only a single prototype of the system was built, the experimentally updated model of the device is coupled to a virtual model of a flexible machine, as discussed in the Numerical investigations for active isolation of flexible machine tools section. Simulation driven investigations for the controlled transmissibility show the actuator to be effective in a frequency range of 1–100 Hz with maximum case specific attenuations of up to 25 dB. These results are instructive for a planned complete experimental characterization as discussed in the Conclusions and outlook section.

Electro-hydraulic actuator working principle

A schematic representation of the machine investigated is shown in Fig. 1(a). The machine is mounted on four actuators. Two actuators support the machine towards the front ($-Z_{MT}$) and two more support the machine towards the rear ($+Z_{MT}$). Machines as these (Fig. 1(a)) are installed in production environments wherein typical floor vibrations levels range from 1 to 50 μm within frequency bands of 1–50 Hz [2,3]. These vibrations excite the low-frequency structural modes of these machines and result in table and/or tool point displacements being potentially greater than the allowable machining and/or measurement deviations. The goal of the controlled electro-hydraulic actuator is to hence reduce the intensity of ground vibrations (g) transmitted to the table (t) and/or to the tool point (q).

Basic elements of the electro-hydraulic system are shown schematically in Fig. 1(b) and constructional details of the actuator are shown in Fig. 1(c). Ground motion experienced by the bridge support results in motion at the machine mounting location (p) as well as at the table (t) and tool point (q) locations. Motion detected by a low-frequency acceleration sensor at the

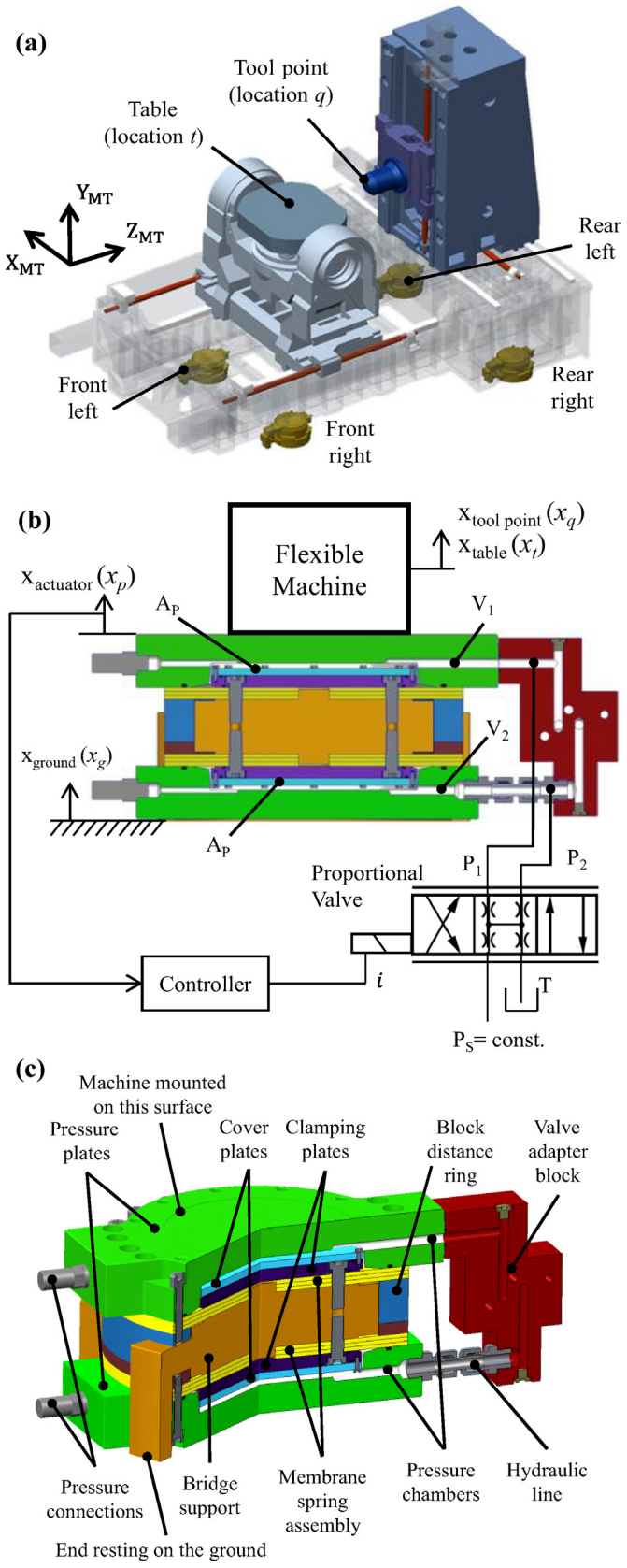

Fig. 1. (a) Schematic representation of a machine mounted on four actuators; (b) schematic of valve controlled electro-hydraulic system; (c) sectional view of the construction of the actuator. Nomenclature in (b) is described in the Modelling the electro-hydraulic actuator dynamics section.

machine mounting location(s) acts as an input to the controller that drives a proportional valve that controls the fluid flow to the actuator. The electro-hydraulic actuator is akin to a double-acting hydraulic cylinder with two different pressure chambers, as shown in Fig. 1(c). Flow to the actuator results in movement of the pressure plates and the machine to counter the motion caused by the ground vibrations. The flow also results in pressure being developed in the chambers which generates a force. This force generated by the actuator may excite the structural modes of the machine that it is supporting. Hence, effective compensation and isolation of ground motion necessitates a complete dynamical model of the electro-hydro-mechanical system, as formulated in the Modelling the electro-hydraulic actuator dynamics, Experimental characterization of actuator dynamics, Numerical investigations for active isolation of flexible machine tools sections.

In the absence of any external disturbance, the actuator behaves like a passive system, with the membrane spring assembly (see Fig. 1(c)) and the hydraulics providing a very high passive stiffness. The device is designed and dimensioned for a static load of up to 4 tonnes [9].

Modelling the electro-hydraulic actuator dynamics

The electro-hydraulic system shown in Fig. 1(b) is a classic example of a valve-controlled piston [11–13]. Dynamics of the main elements are formulated herein to obtain the open-loop transfer function between input to the valve and actuator position output, without considering the structural dynamics of the machine mounted on the actuator, which are separately included in the Numerical investigations for active isolation of flexible machine tools section.

Valve dynamics

An electro-hydraulic proportional valve acts as a high gain electrical to hydraulic transducer. The valve's electronic driver converts the commanded voltage to current. The valve's solenoid converts this current into a mechanical force acting on the spool against a return spring, which in turn results in spool movement and regulation of valve flow. Although valve dynamics are influenced by nozzle and orifice sizes, spring rates, spool diameters, and supply pressure, etc.—that make the valve's response nonlinear, valves are often linearized and can be represented by a second order transfer function as [14,15]:

$$G_{\text{valve}} = \frac{x_v}{v}(s) = K_v\left[\frac{1}{1 + (2\zeta/\omega_{\text{nv}})s + (s/\omega_{\text{nv}})^2}\right] \tag{1}$$

wherein x_v is the valve spool displacement, v is the supplied voltage, K_v is a gain, ω_{nv} is the apparent natural frequency of the valve and ζ is the apparent damping ratio of the valve.

Hydraulic and piston dynamics

Valve flow supplied to the pressure chambers of the actuator results in movement of the pressure plate of the actuators and the machine mounted on the actuator. Assuming valve orifices to be matched and symmetrical under constant supply pressure (P_S), the linearized flow equations are [12]:

$$\begin{aligned} Q_1 &= K_Q x_v - 2K_C P_1 \\ Q_2 &= K_Q x_v + 2K_C P_2 \end{aligned} \tag{2}$$

wherein Q_1 and Q_2 are the forward and return flows in m^3/s and P_1 and P_2 are the forward and return pressures. K_Q corresponds to a valve flow coefficient represented in $m^3/s/mA$ and K_C is the valve flow-pressure coefficient in $m^3/s/Pa$ [15]. Adding the valve flow equations gives:

$$Q_L = K_Q x_v - K_C P_L \tag{3}$$

wherein $Q_L = (Q_1 + Q_2)/2$ is the load flow and $P_L = P_1 - P_2$ is the load pressure difference. Assuming that the pressure in each chamber is uniformly distributed, and that fluid leakage is negligible, application of the continuity equation to each piston chamber yields [12]:

$$\begin{aligned} Q_1 &= \frac{dV_1}{dt} + \frac{V_1}{\beta}\frac{dP_1}{dt} \\ -Q_2 &= \frac{dV_2}{dt} + \frac{V_2}{\beta}\frac{dP_2}{dt} \end{aligned} \tag{4}$$

wherein β is the effective bulk modulus of the hydraulic system. V_1 and V_2 are the volumes of the forward and return chambers, which may be expressed as:

$$\begin{aligned} V_1 &= V_{01} + A_1 x_p \\ V_2 &= V_{02} - A_2 x_p \end{aligned} \tag{5}$$

wherein V_{01} and V_{02} are the initial volumes in each of the chambers and x_p is the displacement of the piston/pressure plates. A_1 and A_2 are the areas of piston, which are identical in the present case, i.e. $A_1 = A_2 = A_P$. Assuming the piston is centred such that: $V_{01} = V_{02} = V_0$, the total volume of fluid under compression in both chambers becomes: $V_t = V_1 + V_2 = 2V_0$.

The volume and continuity equations can be combined, linearized and Laplace transformed by substituting Eq. (5) into Eq. (4) to yield [12]:

$$Q_L = A_p s x_p + \frac{V_t}{4\beta} s P_L. \tag{6}$$

Ignoring the flexibilities of the machine tool system for now (which are considered separately in the Numerical investigations for active isolation of flexible machine tools section), the dynamic equilibrium equation of the actuator piston under an external load can be expressed as:

$$F_p = P_L A_p = Ms^2 x_p + Cs x_p + K_L x_p + F_L \tag{7}$$

wherein F_p is the force generated by the actuator and F_L is the external load on the actuator. Since the actuator (without the machine) is akin to a single degree-of-freedom system, M is the translating mass of the actuator, C is the viscous damping coefficient and F_L corresponds to the static stiffness of the actuator.

Eqs. (3), (6) and (7), when solved simultaneously, results in:

$$x_p = \frac{(K_Q/A_p)x_v - \left(K_C/A_p^2\right)(1 + (V_t/4\beta K_C)s)F_L}{\left(V_t M/4\beta A_p^2\right)s^3 + \left(\left(K_C M/A_p^2\right) + \left(CV_t/4\beta A_p^2\right)\right)s^2 + \left(1 + \left(CK_C/{A_p}^2\right) + \left(K_L V_t/4\beta A_p^2\right)\right)s + \left(K_C K_L/A_p^2\right)}. \tag{8}$$

Under the no load assumption and since typically the critical damping of the membrane spring and actuator is very low, i.e.

$CK_C/A_p^2 \ll 1$, it can be neglected [9,12]. The transfer function, G_{act} between valve and actuator position hence reduces to:

$$G_{act} = \frac{x_p}{x_v} = \frac{(K_Q/A_p)}{\left(s + \left(K_C K_L/A_p^2\right)\right)\left((s^2/\omega_h^2) + (2\delta_h/\omega_h) + 1\right)} \quad (9)$$

wherein $\omega_h = \sqrt{\frac{4\beta A_p^2}{V_t M}}$ is the hydro-mechanical natural frequency and $\delta_h = \frac{K_C}{A_p}\sqrt{\frac{\beta M}{V_t}}$ is the dimensionless hydraulic damping ratio, both of which play a deciding role in the behaviour of the electro-hydraulic actuator.

Eqs. (1) and (9) are combined to obtain the complete open-loop electro-hydraulic transfer function from voltage input to the valve to actuator position output, G_{EHA}:

$$G_{EHA} = \frac{x_p}{v} = G_{valve} G_{act}. \quad (10)$$

The moving mass of the actuator (M), total volume of fluid in chambers (V_t), active area of the piston annulus (A_p) and the designed static stiffness (K_L) are estimated from the CAD model of the developed actuator [9]. Initial values for flow gain (K_Q) and flow-pressure (K_C) coefficients, apparent valve natural frequency (ω_{nv}) and damping ratio (ζ) are available from the valve manufacturer [15]. However, since valve parameters are dependent on operating conditions and are evaluated at constant flow and supply pressure considerations, which are not always guaranteed in real test conditions, these are identified from experiments as discussed in the Experimental characterization of actuator dynamics section. To obtain better confidence in the static stiffness of the actuator (K_L), and since the viscous damping coefficient (C) is not known a priori, these too are identified from experiments.

Experimental characterization of actuator dynamics

A physical prototype of the electro-hydraulic actuator was constructed as shown in Fig. 2. The actuator was controlled by an in-house developed modular platform coupled to a real-time capable digital signal processing board. A hydraulic aggregate (not shown in Fig. 2) capable of delivering more than 100 l/min at pressures up to 200 bar was used. To ensure a constant supply pressure of ~30 bar, an accumulator was installed in the supply line (not shown in Fig. 2), as was also a pressure relief valve such as to protect the actuator.

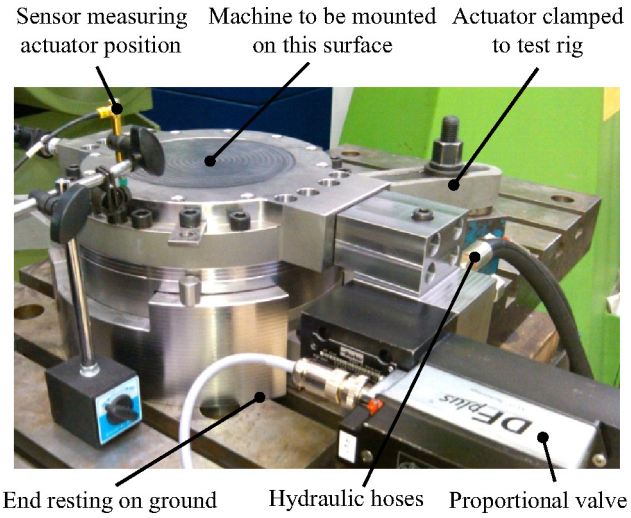

Fig. 2. Physical prototype of the electro-hydraulic actuator.

System identification

The actuator was first operated in its open-loop mode to identify the parameters within Eq. (10). Voltage input to the valve in the form of a linear sine chirp waveform with starting frequency as 0.1 Hz and final frequency as 100 Hz was supplied for a period of 100 s. Actuator position output was measured using an inductive displacement transducer. Response was also measured using an accelerometer mounted on the moving part (accelerometer not shown in Fig. 2). Measured transfer function, i.e. $G_{EHA\ measured}$ was observed to be contaminated by measurement noise. Potential sources of this noise are the dynamic excitations resulting from the clamping/fixture setup that secures the actuator on the experimental test rig. Even though the raw measurement data is averaged over several measurements, it remains noisy. Hence, to retain only the essential measurement information, measured data was filtered using a Savitzky–Golay moving average filter of the second degree [16].

System identification was performed by formulating an objective function that minimizes the difference between the measured and model predicted transfer functions [17], i.e. $G_{EHA\ measured}$ and $G_{EHA}(x_d)$. The objective function takes the form of minimizing the sum of square of the residuals r_i:

$$\min f_{objs}(x_d) = \sum_{i=1}^{n_p} r_i^2 \text{ such that } lb \le x_d \le ub \quad (11)$$

wherein the residual is: $r_i = G_{EHA\ measured} - G_{EHA}(x_d)$ at each frequency point i for a total of n_p points; lb and ub represent the lower and upper bounds on the set of model parameters to be identified, x_d. This set includes the static stiffness (K_L), flow gain (K_Q) and flow-pressure (K_C) coefficients, apparent valve natural frequency (ω_{nv}), damping ratio (ζ) and the viscous coefficient of the actuator (C), such that $x_d \subset \{K_L; C; \omega_{nv}; \zeta; K_Q; K_C\}$. Actuator spring stiffness is bound to be within ±50% of its designed value. The apparent valve natural frequency, flow gain and flow-pressure coefficients are bound by the realizable range of operating parameters for the valve [15]. Apparent valve damping ratio is bound by ranges typical for proportional and/or servo valves [14].

All actuator, valve and hydraulic system data including starting and identified values for the set of x_d are listed in Table 1. Identified set of parameters are obtained by solving the optimization problem of Eq. (11) using the sequential quadratic programming method. The set of identified parameters are non-unique and were observed to be dependent on starting values. However, comparison of measured open-loop transfer function (between input to the valve and actuator output position) with model predicted transfer function with identified parameters in Fig. 3 shows a good match, and the model is hence deemed satisfactory.

The roll-off in the open-loop response seen in Fig. 3 is typical of valve-controlled pistons acting against a load spring that result in low frequency lag at $K_C K_L/A_p^2$ rad/s which becomes a true integration at $K_L = 0$ [12]. The differences in phase between the identified model and measured behaviour at higher frequencies can be attributed to the nonlinearities of the flow-pressure characteristics of the valve that may result in the hydraulic damping ratio (δ_h) changing as a function of frequency [12]. These flow-pressure characteristics, especially the valve flow-pressure coefficient (K_C) are a strong function of the changing operating parameters and leakages, both of which are neglected in the linearized model considered.

This experimentally updated model is used to virtually investigate the controlled closed-loop reference tracking transfer function of the electro-hydraulic actuator. A PID controller was implemented and the resulting closed-loop tracking transfer function is shown in Fig. 4.

Table 1
Actuator, valve and hydraulic system data.

	Variable description	Symbol	Value	
			Starting value	Identified value
Actuator data–estimated from CAD model [9]	Moving mass	M [kg]	56	–
	Active area of piston	A_p [m^2]	3.10×10^{-2}	–
	Viscous coefficient*	C [Ns/m]	3900	1951
	Total chamber volume	V_t [m^3]	5.39×10^{-4}	–
	Actuator static stiffness*	K_L [N/m]	6.8×10^8	6.8×10^8
Proportional valve D3FP series [14,15]	Flow gain coefficient*	K_Q [m^3/s/mA]	9.74×10^{-6}	1.94×10^{-6}
	Flow pressure coefficient*	K_C [m^3/s/Pa]	7.15×10^{-11}	6.6×10^{-11}
	Natural frequency*	ω_{nv} [rad/s]	628	524
	Damping ratio*	ζ	0.48	0.65
	Gain	K_v	2	–
Hydraulic fluid property	Bulk modulus of fluid	β [N/m^2]	1.4×10^9	–

* Parameters identified from experiments.

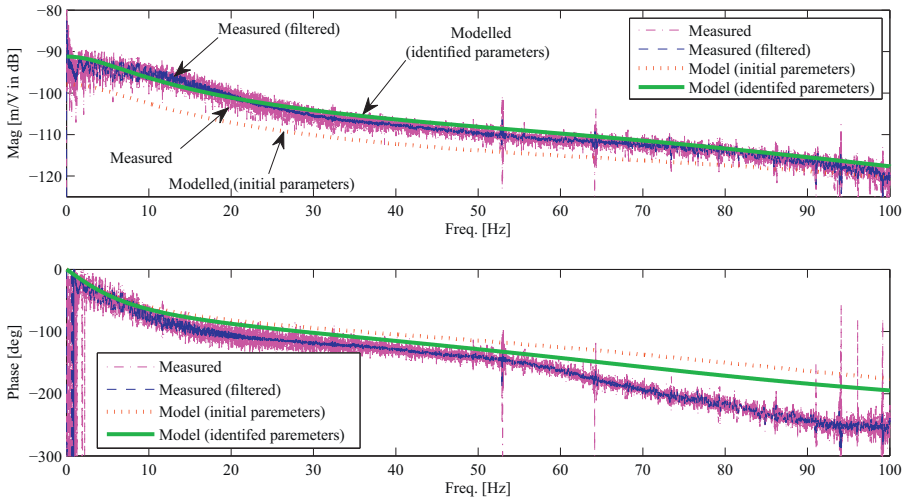

Fig. 3. Comparison of open-loop experimental and modelled transfer function between input to the valve and actuator output position with initial and identified parameters.

The actuator has a bandwidth of ~95 Hz (corresponding to a 3 dB drop in response). The hydro-mechanical natural frequency at ω_h = ~2180 Hz is much higher than the valve natural frequency identified as ω_{nv} = ~84 Hz. This suggests that the response of the valve-controlled actuator is limited by the dynamics of the valve. Closed loop response in Fig. 4 is for the case of the actuator without the machine. For the case of the actuator supporting a flexible machine that has structural frequencies lower than valve natural frequency, controller performance will be limited by the lowest natural frequency that occurs within the control loop. Hence, the low-frequency machine tool structural resonances that will potentially dominate the frequency response of the valve-controller actuator must necessarily be considered in the controlled system design, as is discussed in the Numerical investigations for active isolation of flexible machine tools section.

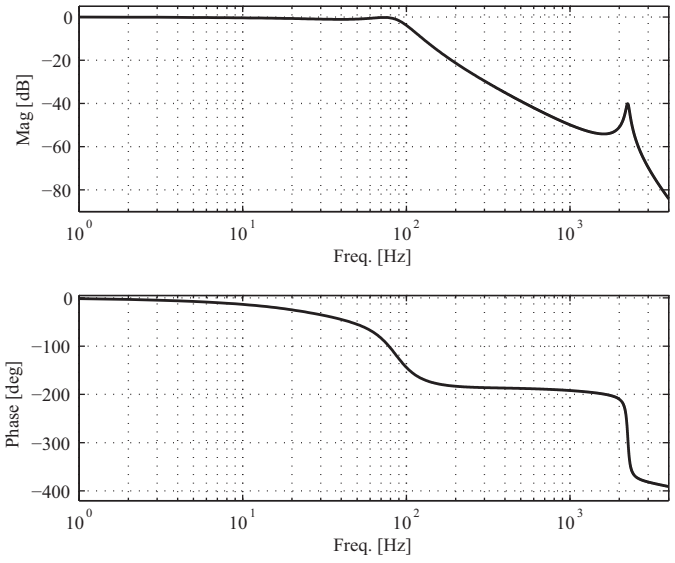

Fig. 4. Simulated closed-loop reference tracking transfer function for the controlled electro-hydraulic actuator.

Numerical investigations for active isolation of flexible machine tools

A single prototype of the system was built, and hence it was not possible to test the device with a real machine, since that would require as many actuators as machine mounting/supporting points. Instead, the experimentally updated model of the actuator is coupled to a finite element model of a machine to numerically investigate isolation. The machine model investigated is schematically shown in Fig. 1(a). Its dynamical model has been previously validated elsewhere in [18].

Modelling actuator dynamics and transmissibility for a flexible machine tool

Structural modes of the machine under investigation are well below the valve natural frequency and the hydro-mechanical natural frequency of the actuator supporting the machine

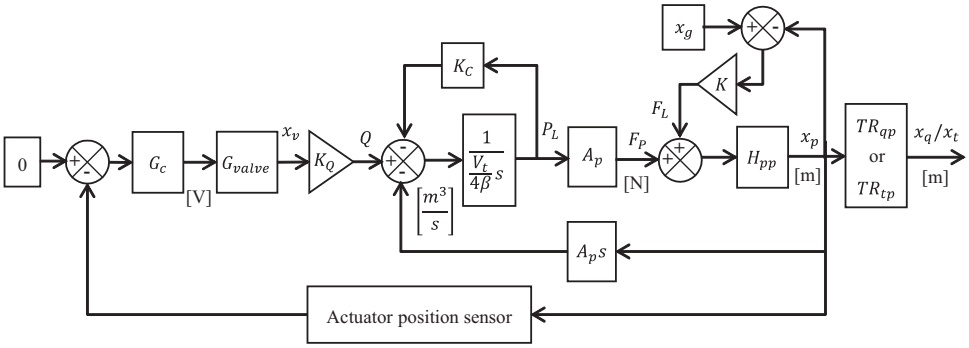

Fig. 5. Block diagram level description of controlled transmissibility. (G_C is the controller, G_{valve} represents the valve dynamics, K_Q and K_C are the valve flow and pressure coefficients, Q is the valve flow, V_t is the total volume of fluid in the chambers, β is the bulk modulus of the fluid, A_p is the area of the pressure chamber, P_L is the load pressure, K is a combination of the load and hydraulic stiffness of the actuator, F_p and F_L are the forces generated by the actuator and the disturbance forces respectively, H_{pp} is the direct driving point receptance at each of the actuator mounting locations, x_p is the actuator position, TR_{qp}, TR_{tp} are the displacement transmissibilities, x_q and x_t are the controlled tool and table positions, and x_g is the ground motion).

($\omega_h = \sqrt{\frac{4\beta A_p^2}{V_t M_t/4}} = \sim 257$ Hz for the machine weight of $M_t = \sim 16$ t supported on four mounts). The force generated by the actuator (F_p) may excite these structural modes resulting in these modes dominating the closed-loop dynamics of the valve-controlled actuator.

These structural dynamics are described by a transfer function between the applied force (F_p) and the actuator position (x_p), as:

$$\frac{x_p}{F_p} = H_{pp}(\omega) \tag{12}$$

wherein $H_{pp}(\omega)$ is the direct driving point receptance, i.e. the displacement-to-force frequency response function (FRF) of the machine under investigation, obtained as describe below.

The force generated by the actuator ($F_p = P_L A_p$) also acts against the ground motion that results in a disturbance like force:

$$F_L = K(x_g - x_p) \tag{13}$$

wherein x_g is the ground motion, x_p is the actuator position and $K = K_L + K_h$ is a combination of the load (K_L) and hydraulic stiffness $\left(K_h = \frac{4\beta A_p^2}{V_t}\right)$.

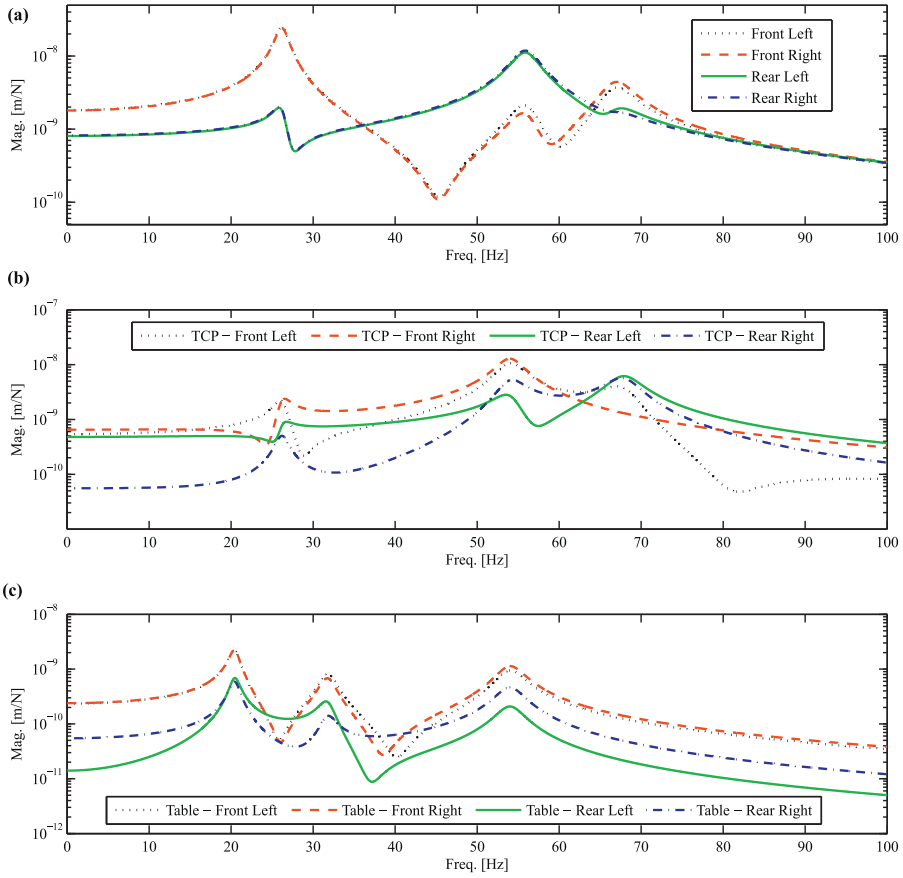

Fig. 6. (a) Direct driving point receptances (H_{pp}) in the vertical (Y_{MT}) direction for each of the four machine mounting locations (b) cross receptances (H_{qp}) between the tool point (TCP) and each of the machine mounting locations in the vertical (Y_{MT}) direction (c) cross receptances (H_{tp}) between the table and each of the machine mounting locations in the vertical (Y_{MT}) direction.

Table 2
Response of the machine in the principal Y_{MT} direction at the actuator locations.

Freq. [Hz]	Motion	Values of the undamped mass normalized modal vector ($\Phi_{Y_{MT}}$) at actuator locations			
		Front left	Front right	Rear left	Rear right
20	Yaw	−0.0434	−0.0441	0.0139	0.0119
26	1st Torsion	0.20	−0.198	−0.0493	0.05
31	Heave	−0.0224	−0.0183	−0.006	−0.004
56	2nd Torsion	0.12	−0.10	−0.286	0.29
68	Pitch	0.0713	0.0004	−0.116	−0.107

The dynamic equilibrium for the multiple degree-of-freedom machine results in a modified form of Eq. (7) which is more convenient to describe using a block diagram level description of the valve-controlled actuator supporting a flexible machine, as shown in Fig. 5. The machine is mounted on four different active mounts, each of which will react differently to excitation and the load dynamics, resulting a multiple-input-multiple-output (MIMO) system. The schematic representation in Fig. 5 however, is for a simplified single-input–single-output (SISO) model of each of the four actuators separately supporting the machine and acting against ground motion.

Since the isolator counters ground motion by moving the flexible machine mounted onto it, it becomes necessary to evaluate the transmissibility from ground motion to table and/or tool point motion. This transmissibility function is decomposed into two parts, the transmissibility from the ground to the actuator TR_{pg} and the transmissibility from the actuator to the table and the tool point, i.e. TR_{tp} and TR_{qp} respectively, as shown schematically in Figs. 1(a) and 5. Evaluating TR_{pg} is straightforward using Eq. (12) and F_P and F_L (see Fig. 5). The relationship between actuator and table and/or tool point motion on the other hand is more involved and can be described using a frequency dependent transmissibility function:

$$TR_{tp}(\omega) = \frac{x_t(\omega)}{x_p(\omega)} = \frac{H_{tp}(\omega)}{H_{pp}(\omega)} = \frac{(x_t(\omega)/F_p(\omega))}{(x_p(\omega)/F_p(\omega))}; \quad p = 1,\ldots,4$$
$$TR_{qp}(\omega) = \frac{x_q(\omega)}{x_p(\omega)} = \frac{H_{qp}(\omega)}{H_{pp}(\omega)} = \frac{(x_q(\omega)/F_p(\omega))}{(x_p(\omega)/F_p(\omega))}; \quad p = 1,\ldots,4 \tag{14}$$

wherein $H_{tp}(\omega)$ and $H_{qp}(\omega)$ represent the displacement-to-force cross FRFs between actuator location and table and tool centre point (TCP) positions. $H_{pp}(\omega)$ is the direct driving point FRF at the actuator location, as expressed above in Eq. (12).

These FRFs (in Eqs. (12) and (14)) are constructed using the mass normalized eigenvectors and eigenvalues output from a modal analysis run carried out using the virtual model of the machine from the finite element environment, as:

$$H_{ij}(\omega) = \sum_{r}^{N_m} \frac{\Phi_{ir}\Phi_{jr}}{-\omega^2 + i_m 2\zeta_r \omega\omega_{nr} + \omega_{nr}^2} \tag{15}$$

wherein ω_n is the undamped eigenvalue for r modes of interest for a total of N_m modes; $\Phi_{i,j}$ is the eigenvector at the location and direction of interest (i and j are the respective response and excitation locations); ζ_r is the modal damping ratio; ω is the frequency vector and i_m is the imaginary operator.

Direct driving point receptances/FRFs (H_{pp}) for each of the machine mounting locations as well as cross receptances/FRFs between the table and tool point, and each of the machine mounting locations, i.e. H_{tp} and H_{qp} are shown in Fig. 6(a–c), respectively. Since the actuator can only counter ground motion in the vertical direction, response comparisons in Fig. 6 are limited to the Y_{MT} directional response. However, cross response between the actuator vertical motion (Y_{MT}) and response at the TCP/Table in the other principal horizontal directions (X_{MT}, Z_{MT}) is also considered in the analyses of transmissibilities. Response comparisons are limited to the low-frequency structural modes of the machine that

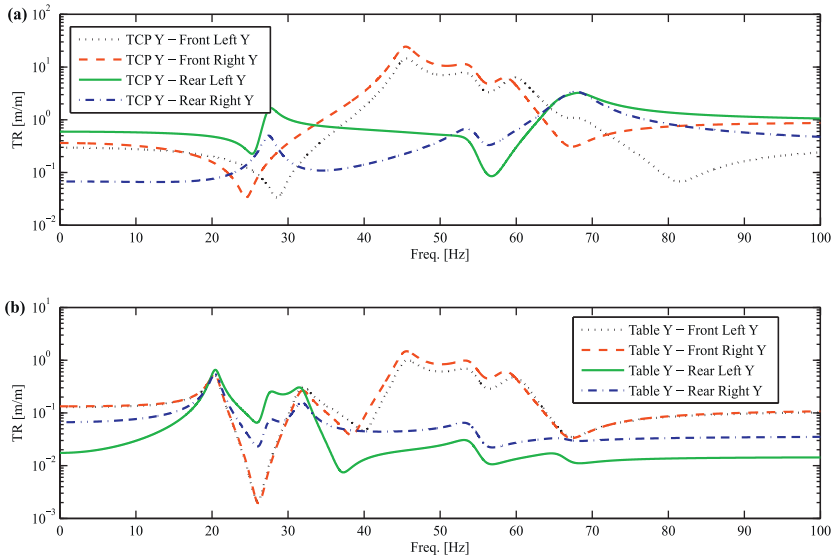

Fig. 7. Transmissibility functions between: (a) motion at each mounting location and the tool point (TCP), i.e. TR_{qp} in the vertical (Y_{MT}) direction, and (b) motion at each mounting location and the table, i.e. TR_{tp} in the vertical (Y_{MT}) direction.

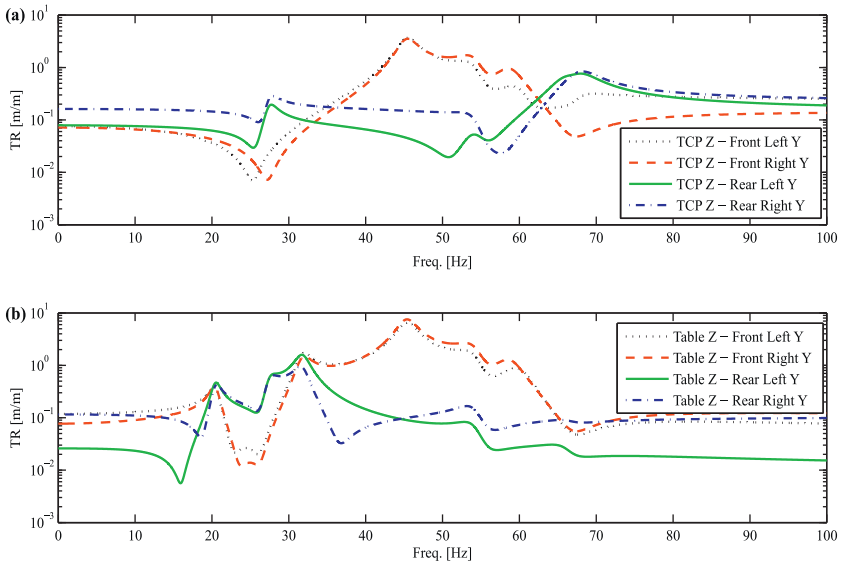

Fig. 8. Cross transmissibility functions between: (a) motion at each mounting location in the vertical (Y_{MT}) direction and the tool point (TCP) in the horizontal (Z_{MT}) direction, i.e. TR_{qp}, and (b) motion at each mounting location in the vertical (Y_{MT}) direction and the table, i.e. TR_{tp} in the horizontal (Z_{MT}) direction.

may get excited due to ground vibrations in the frequency band of 1–100 Hz.

As evident from Fig. 6(a), the front mounts respond differently as compared to the rear mounts. The modes at ~26 Hz and at ~56 Hz correspond to the first two torsional modes of the machine and the mode at ~68 Hz corresponds to a pitching mode. The cross receptances between the tool and the mounting locations (Fig. 6(b)) as well as in between the table and each of the mounting locations (Fig. 6(c)) are different than the driving point receptances (Fig. 6(a)). This is because cross receptances include modes that are excitable and observable between the table and/or the tool point, and each of the mounting locations. The mode at ~20 Hz in Fig. 6(c) corresponds to a yaw motion, whereas the mode at ~31 Hz corresponds to a heaving motion. These mode shapes as seen at the driving point (location q in Fig. 1) are described in Table 2 using the values of the undamped mass normalized modal vectors at these locations.

Transmissibilities in the vertical (Y_{MT}) directions evaluated as per Eq. (14) are shown in Fig. 7(a–b). These transmissibilities have been evaluated by first decomposing each of the receptances within Eq. (14) to the Laplace domain ($i_m\omega \rightarrow s$). Similarly, cross transmissibilities between actuator motion in the vertical (Y_{MT}) direction and motion at the TCP/Table in the other principal horizontal directions (X_{MT}, Z_{MT}) is also shown in Figs. 8 and 9. Fig. 8 shows the cross transmissibilities between actuator vertical (Y_{MT}) motion and TCP/Table motion in the horizontal (Z_{MT}) direction. Fig. 9 shows the cross transmissibilities between actuator vertical (Y_{MT}) motion and TCP/Table motion in the horizontal (X_{MT}) direction.

As evident from Figs. 7–9, transmissibility functions between motion at each mounting location and the tool point, i.e. TR_{qp} are

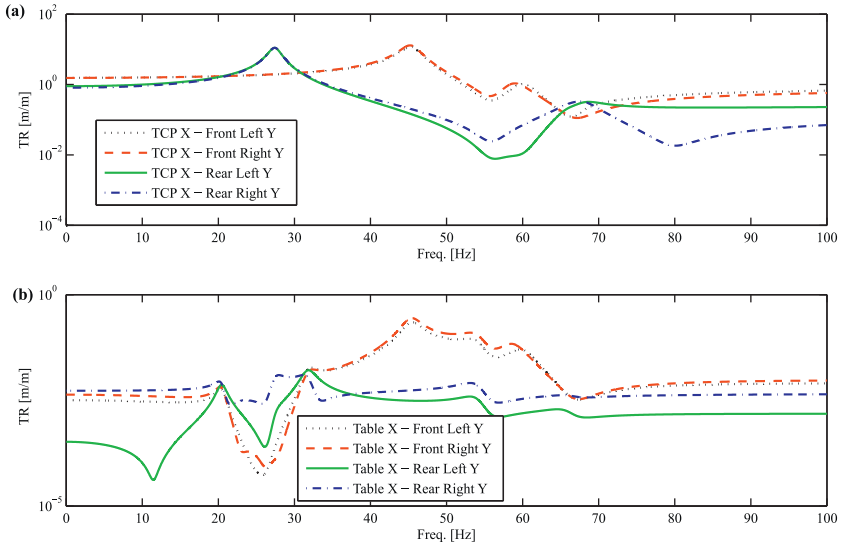

Fig. 9. Cross transmissibility functions between: (a) motion at each mounting location in the vertical (Y_{MT}) direction and the tool point (TCP) in the horizontal (X_{MT}) direction, i.e. TR_{qp}, and (b) motion at each mounting location in the vertical (Y_{MT}) direction and the table, i.e. TR_{tp} in the horizontal (X_{MT}) direction.

different than the transmissibility functions between motion at each mounting location and the table, i.e. TR_{tp}. Further differences between direct and cross transmissibilities are also noticeable from Figs. 7–9. Cross transmissibilities (Figs. 8 and 9) are approximately an order of magnitude lower than the direct transmissibilities (Fig. 7). Since the isolator must necessarily reduce dynamic excitations transmitted to the tool point and the table, as well as maintain the relative isolated deformations between the table and tool point within permissible levels, controlled isolation of the electro-hydraulic actuator is investigated for reducing all these transmissibilities, as discussed in the Controlled transmissibility section.

Moreover, as is evident from Figs. 6–9 and Table 2, since the response and transmissibilities are different at each of the mounting locations, a decentralized control approach is preferred presently because of its ease of implementation. In decentralized control, each actuator is operated independently by simply feeding back signal proportional to the corresponding response at that location. Since each actuator and sensor pair is collocated, it also makes for easy tuning of each controller separately. Such a decentralized control strategy also allows for control actions to respond to spectral and spatial variations in ground vibrations when the ground vibrates with a waveform that result in each mounting location being excited differently.

Controlled transmissibility

A MATLAB Simulink model is developed in line with the block diagram in Fig. 5. A simple PI controller with/without a compensator was implemented, and the controlled transmissibilities are shown in Fig. 10 for the representative case of transmissibilities between ground motion (x_g) detected at the front left actuator and the tool point (x_q) in the vertical (Y_{MT}) direction only. As evident in Fig. 10, a simple PI controller is effective in attenuating transmissibilities only up to frequencies of

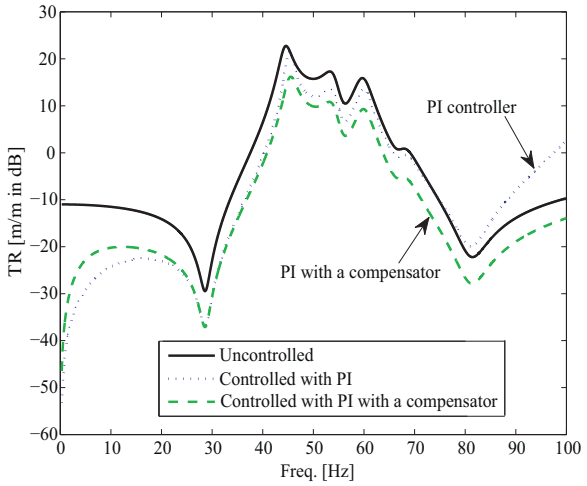

Fig. 10. Simulated controlled displacement transmissibility (TR_{qg}) between ground motion (x_g) and the tool point (x_q) in the vertical (Y_{MT}) direction for the front left actuator.

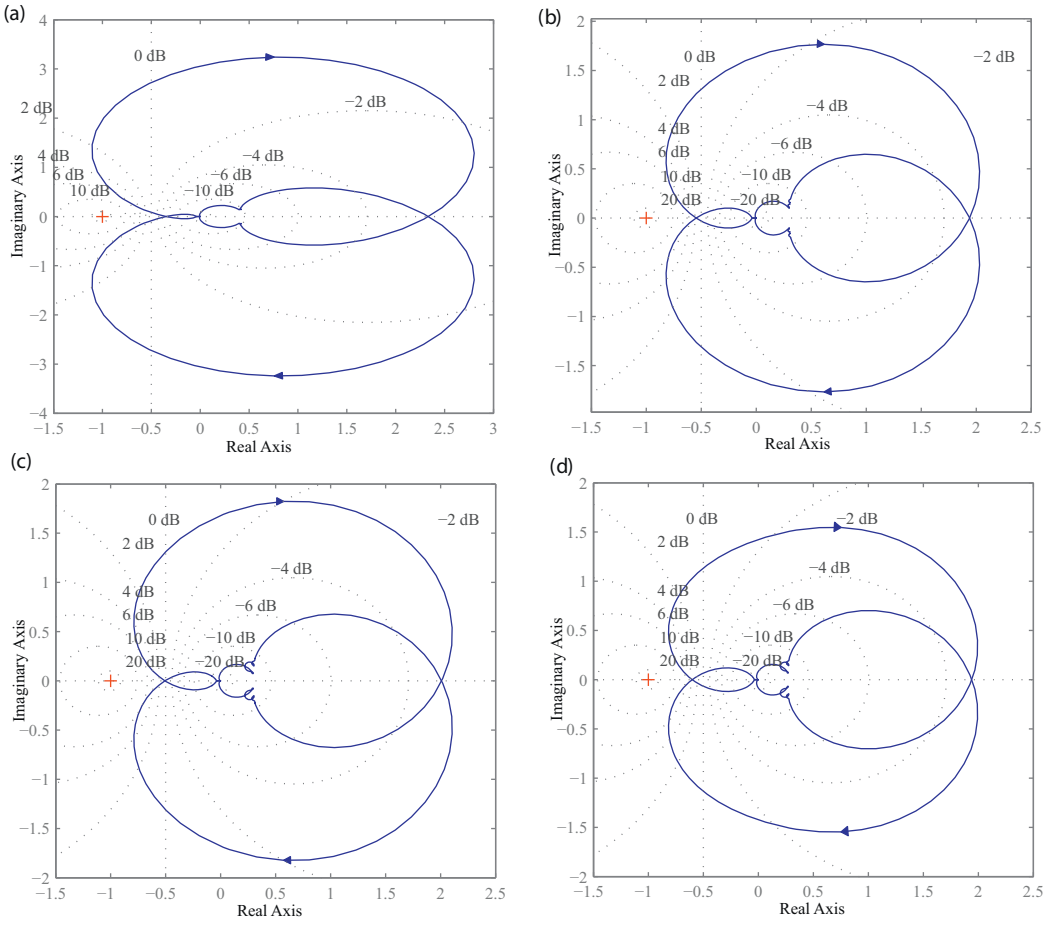

Fig. 11. Nyquist plots showing closed loop stability for controlling the: (a) front left actuator, (b) front right actuator, (c) rear left actuator, (d) the rear right actuator.

~70 Hz, beyond which range transmissibility was amplified instead of being isolated. This PI controller when supplemented with a compensator shows consistent isolation in the full frequency range of interest, i.e. up to 100 Hz. Seeing that the PI controller with a compensator results in consistent attenuation of transmissibilities, and even though it has poorer low-frequency isolation compared to the simple PI controller, it is adopted as the preferred control strategy.

Controlled transmissibility is investigated separately for each of the four active mounts. Closed-loop response for the controlled actuator supporting the machine at all locations was observed to be stable, as evident from the Nyquist plots characterizing closed loop stability in Fig. 11.

As evident in Fig. 11, closed loop response for the controlled actuator supporting the machine at all locations is stable since there is no encirclement of critical '−1, 0' stability point on the complex plane. Gain and phase margins evaluated from these Nyquist plots range from 4 to 14 dB and 30–36°, respectively (depending on actuator location). The corresponding gain crossover frequencies range from 215 to 221 Hz, with phase cross over frequencies of ~397 Hz. These margins suggest that marginal improvement of controlled transmissibility is yet possible using an advanced and/or a well-tuned controller.

Using the PI controller with a compensator, the simulated controlled transmissibilities between ground motion (x_g) at all four actuator locations and the table (x_t), and between ground motion (x_g) at all four actuator locations and the tool point (x_q), i.e. TR_{tg} and TR_{qg} were evaluated, and are shown in Figs. 12 and 13, respectively. The transmissibilities in Figs. 12 and 13 are for the case of ground motion and response only in the machine vertical direction, i.e. Y_{MT}.

From Fig. 12 it is clear that the isolator can consistently attenuate transmissibilities between the ground and table for the full frequency range of interest. Low-frequency attenuation ranges from ~25 dB at 1 Hz to ~10 dB between 5 and 10 Hz. Modes

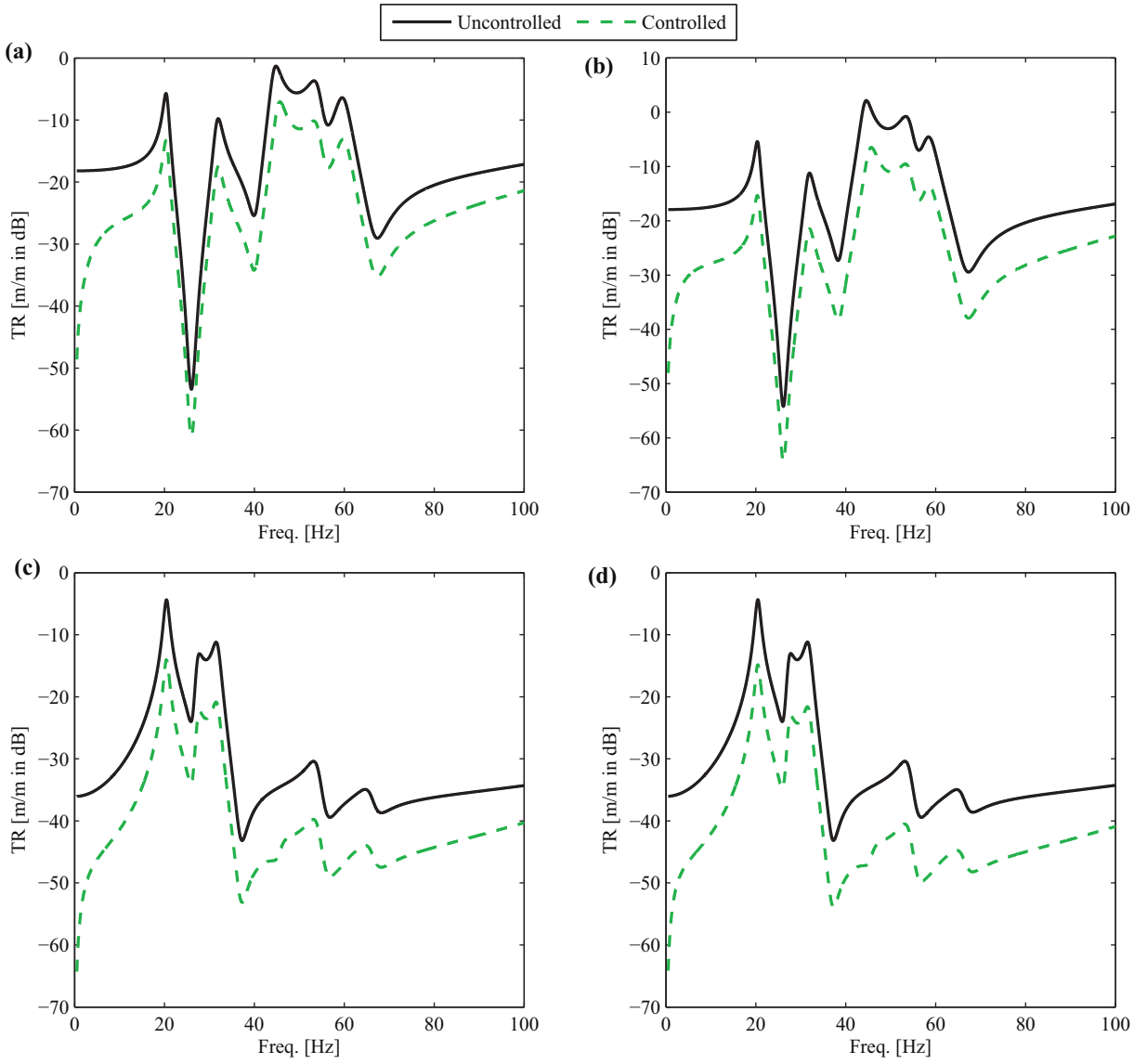

Fig. 12. Simulated controlled displacement transmissibility (TR_{tg}) between ground motion (x_g) and the table (x_t) in the vertical (Y_{MT}) direction. (a) TR_{tg} for the front left actuator, (b) TR_{tg} for the front right actuator, (c) TR_{tg} for the rear left actuator, (d) TR_{tg} for the rear right actuator.

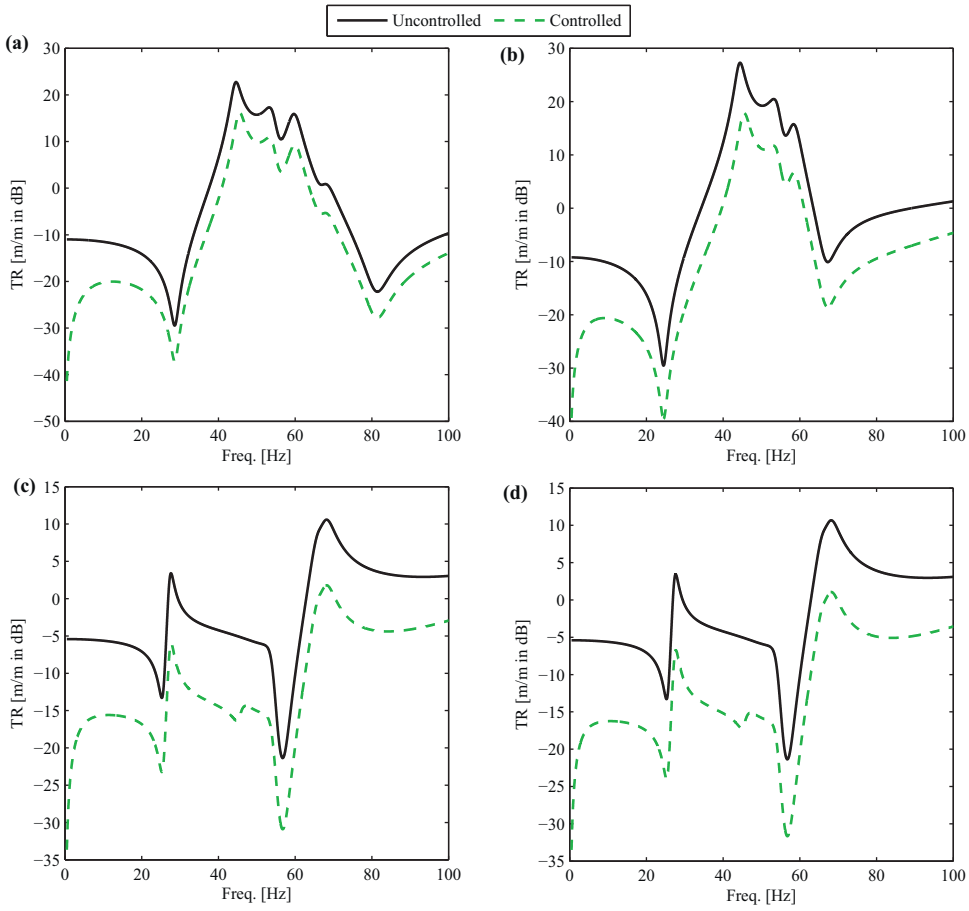

Fig. 13. Simulated controlled displacement transmissibility (TR_{qg}) between ground motion (x_g) and the tool point (x_q) in the vertical (Y_{MT}) direction. (a) TR_{qg} for the front left actuator, (b) TR_{qg} for the front right actuator, (c) TR_{qg} for the rear left actuator, (d) TR_{qg} for the rear right actuator.

between 20 and 60 Hz are all attenuated by 5–10 dB, with slightly higher attenuation of transmissibilities between the rear locations and the table than the front locations and the table. Response between 60 and100 Hz is less attenuated, with maximum attenuation of only ~4 dB between the front locations and the table and slightly better attenuation of ~6 dB between the rear locations and the table.

Comparable to reductions in transmissibilities between the ground and table, there is also a noticeable reduction in transmissibilities between ground and tool point, as evident in Fig. 13. The low-frequency attenuation in this case ranges from ~20 dB at 1 Hz to ~10 dB between 5 and10 Hz. Transmissibility of the mode at ~26 Hz (Fig. 13(c–d)) is attenuated by ~10 dB. Transmissibility of the mode at ~45 Hz between the front left location and the tool point is attenuated by ~7 dB (Fig. 13(a)) and by ~10 dB between the front right location and the tool point (Fig. 13(b)). Transmissibility between 60 and100 Hz in this case too is less attenuated between the front locations and the tool point (~5 dB) than the rear locations and the tool point (~7 dB).

Since the actuator is designed to respond to ground vibrations only in the vertical (Y_{MT}) direction, any ground motion in the other planar (X_{MT}, Z_{MT}) directions is not detected by the actuator and is transferred to the TCP/Table without being isolated and/or amplified. The actuator is symmetric in construction in each of its planar (X_{MT}, Z_{MT}) directions. Measured behaviour of the actuator in either of its planar directions show the actuator dynamics to be dominated by its lowest frequency mode at ~450 Hz that has a dynamic stiffness of ~200 N/μm. This high dynamic stiffness and natural frequency of the actuator will result in the actuator transmitting low-frequency ground motion in either of the planar directions to the TCP/Table without significantly altering it.

Though the actuator cannot respond to any ground motion in any of the planar directions, it still attenuates the cross transmissibilities between ground motion in the vertical (Y_{MT}) direction and response at the TCP/Table in the horizontal (X_{MT}, Z_{MT}) directions. These attenuations, shown in Fig. 14, are only due to the controlled movement of the actuator in the vertical direction.

Levels of attenuation observed in the direct transmissibilities (Figs. 12 and 13) are similarly observed in the cross transmissibilities, with attenuations ranging from ~20 dB at the low frequencies, and ~5–7 dB at the higher frequencies. Though cross transmissibilities shown in Fig. 14 are for the representative case of controlled action of the front left actuator supporting the machine and responding to ground motion at the same location, similar levels of attenuation were observed for all other machine mounting locations. From attenuations observed in Figs. 12–14, it naturally follows that the relative deformations between the table and tool point can also be attenuated with the use of the electro-hydraulic actuator.

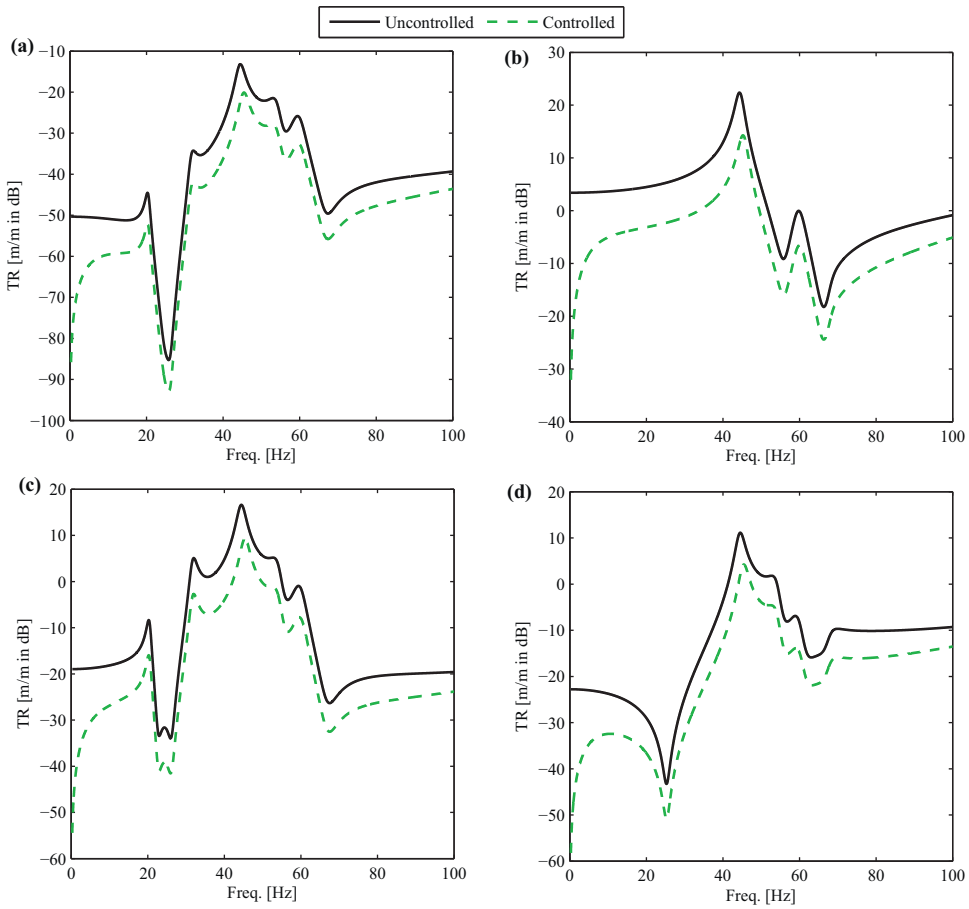

Fig. 14. Simulated controlled displacement transmissibility between ground motion (x_g) in the vertical (Y_{MT}) direction detected at the front left mount and: (a) the table (x_t) in the horizontal (X_{MT}) direction, (b) the tool point motion (x_q) in the horizontal (X_{MT}) direction, (c) the table (x_t) in the horizontal (Z_{MT}) direction, and, (d) the tool point motion (x_q) in the horizontal (Z_{MT}) direction.

Conclusions and outlook

A novel electro-hydraulic actuator was shown effective in being able to isolate machine tools from ground vibrations. The actuator is a classic example of a valve-controlled piston, with flow to the actuator being regulated to move it and the machine that it supports to compensate for ground motion experienced by the machine. Isolation was demonstrated by coupling an experimentally updated actuator model to a virtual model of a machine supported on four active mounts. Decentralized feedback control, because of its easier implementation and tuning was implemented to control each actuator independently of the others, thus allowing the actuator to respond to spectral and spatial variations in ground vibrations. Actuator bandwidth of ~95 Hz allows for controlled transmissibilities between ground, table and the tool point to be well attenuated in the full frequency range of interest from 1 to 100 Hz, with case specific attenuations ranging from 5 to 25 dB.

Like any other isolation solution, the proposed solution is not without limitations. Though the dynamical models developed are generalizable and even though the actuator is designed to be used with an array of different machines, a different machine will result in a different closed loop electro-hydro-mechanical dynamical system, for which control and its parameters need to be designed and tuned independently. Furthermore, potential cross coupling between different actuators and its effect on the stability of the system needs to be further investigated. Stress-testing the proposed system for fatigue life also needs further experimentation. Experimental characterization is also a function of noise-free measurements of low-frequency ground vibrations, which is a known challenge. Advanced control strategies implementing MIMO control laws and/or frequency dependent controllers that also factor in adverse effects of delays, if any, have the potential of further attenuating the controlled transmissibilities, and their implementation forms part of the planned future work.

Despite some of the limitations, results obtained herein are instructive and provide guidelines for a planned complete experimental characterization of a machine under real test conditions. Since the actuator is also a force generator, it can be used as a shaker/exciter to obtain transmissibilities that need to be then controlled and isolated. Though the isolator was shown effective to isolate the effect of ground excitation on the machine, it can also act to isolate vibrations transmitted from the machine to the ground.

Acknowledgments

This research was supported by the Fraunhofer Gesellschaft's ICON Project for Strategic Research Co-Operation on Sustainable Energy Technologies.

References

[1] DeBra, D.B., 1992, Vibration isolation of precision machine tools and instruments, Ann CIRP, 41:711–718.
[2] Rivin, E., 1995, Vibration isolation of precision equipment, Precis Eng, 17:41–56.
[3] Rivin, E., 2006, Vibration isolation of precision objects, Sound Vib, 40:12–20.
[4] Okwudire, C., Lee, J., 2013, Minimization of the residual vibrations of ultra-precision manufacturing machines via optimal placement of vibration isolators, Precis Eng, 37:425–432.

[5] Preumont, A., Horodinca, M., Romanescu, I., de Marneffe, B., Avraam, M., Deraemaeker, A., Bossens, F., Abu Hanieh, A., 2007, A six-axis single-stage active vibration isolator based on Stewart platform, J Sound Vib, 300:644–661.
[6] Kumar, G. Satheesh, Nagarajan, T., 2012, Reconfigurable Stewart platform for vibration isolation, trends in intelligent robotics, automation, and manufacturing, Commun Comput Inf Sci, 330:37–45.
[7] Huang, X., Elliott, S.J., Brennan, M.J., 2003, Active isolation of a flexible structure from base vibration, J Sound Vib, 263:357–376.
[8] Choi, Y.T., Wereley, N.M., Jeon, Y.S., 2005, Semi-active vibration isolation using magnetorheological isolators, J Aircr, 42:1244–1251.
[9] Bischoff, M., 2009, Entwicklung eines aktiven Aufstellelementes zur Schwingungsisolierung von Werkzeugmaschinen, Hochschule für Technik, Wirtschaft und Kultur Leipzig, German. (Masterarbeit).
[10] Abicht, C., Ulbrich, H., Riebe, S., 2002, Active vibration isolation of a Stewart-platform using high response hydraulic actuators, in: Proceedings of the Sixth Int. Conference on Motion and Vibration Control.
[11] Wabner, M., Law, M., Ihlenfeldt, S., 2014, Dynamic modelling of an electro-hydraulic actuator to isolate machine tools from ground vibrations, Proc. of the 11th Int. Conference on High Speed Machining, HSM 2014 (Czech Republic), .
[12] Merritt, H.E., 1967, Hydraulic Control Systems, John Wiley & Sons, NY.
[13] The Mechatronics Handbook. 2007, The Mechatronics Handbook, CRC Press, Boca Raton, FL.
[14] Moog Controls Inc.. 1965, Transfer Functions for Moog Servovalves, Technical Bulletin, Moog Controls Inc., East Aurora, NY.
[15] Parker. 2011, Direct Operated Proportional DC Valve, Series D3FP, Technical Catalogue, Parker, UK.
[16] Orfanidis, Sophocles J., 1996, Introduction to Signal Processing, Prentice Hall, Englewood Cliffs, NJ.
[17] Jelali, M., Kroll, A., 2003, Hydraulic Servo-Systems, Modelling, Identification and Control, Springer-Verlag, London.
[18] Neugebauer, R., Scheffler, C., Wabner, M., Zwingenberger, C., 2011, Advanced calculation of static and dynamic stiffness in mechatronic machine tools, Int J Mechatron Manuf Syst, 4:370–384.